A simple yet stable molybdenum(0) carbonyl complex for upconversion and photoredox catalysis

Winald R. Kitzmann[a], Maria-Sophie Bertrams[a], Pit Boden[b], Alexander C. Fischer[a], René Klauer[a], Johannes Sutter[c], Robert Naumann[a], Christoph Förster[a], Gereon Niedner-Schatteburg[b], Nicolas H. Bings[a], Johannes Hunger[c], Christoph Kerzig[a], Katja Heinze[a,*]

a W. R. Kitzmann, M.-S. Bertrams, A. C. Fischer, R. Klauer, Dr. R. Naumann, Dr. C. Förster, Prof. Dr. N. H. Bings, JProf. Dr. C. Kerzig, Prof. Dr. K. Heinze, Department of Chemistry, Johannes Gutenberg-University of Mainz, Duesbergweg 10–14, 55128 Mainz, Germany; E-Mail: katja.heinze@uni-mainz.de

b Dr. P. Boden, Prof. Dr. G. Niedner-Schatteburg, Department of Chemistry and Research Center Optimas, RPTU Kaiserslautern, Erwin-Schrödinger-Straße 52, 67663 Kaiserslautern-Landau, Germany

c J. Sutter, Dr. J. Hunger, Max-Planck-Institute for Polymer Research, Ackermannweg 10, 55128 Mainz, Germany

KEYWORDS: carbonyl complexes • upconversion • photocatalysis • phosphorescence • metal-to-ligand charge transfer • molybdenum

ABSTRACT: Photoactive complexes with earth-abundant metals have attracted increasing interest in the recent years fueled by the promise of sustainable photochemistry. However, sophisticated ligands with complicated syntheses are oftentimes required to enable photoactivity with non-precious metals. Here, we combine a cheap metal with simple ligands to easily access a photoactive complex. Specifically, we synthesize the molybdenum(0) carbonyl complex $Mo(CO)_3$(tpe) featuring the tripodal ligand tris(pyridyl)ethane (tpe) in two steps with high overall yield. The complex shows intense deep-red phosphorescence with excited state lifetimes of several hundred nanoseconds. Time-resolved infrared spectroscopy and laser flash photolysis reveal a triplet metal-to-ligand charge-transfer (^{3}MLCT) state as lowest excited state. Temperature-dependent luminescence complemented by density functional theory (DFT) calculations suggest thermal deactivation of the ^{3}MLCT state *via* higher lying metal-centered states in analogy to the well-known photophysics of $[Ru(bpy)_3]^{2+}$. Importantly, we found that the title compound is very photostable due to the lack of labilized Mo–CO bonds (as caused by *trans*-coordinated CO) in the facial configuration of the ligands. Finally, we show the versatility of the molybdenum(0) complex in two applications: (1) green-to-blue photon upconversion *via* a triplet-triplet annihilation mechanism and (2) photoredox catalysis for a green-light driven dehalogenation reaction. Overall, our results establish tripodal carbonyl complexes as a promising design strategy to access stable photoactive complexes of non-precious metals avoiding tedious multi-step syntheses.

Introduction

The development of photoactive metal complexes with earth-abundant metals holds great promise to enable sustainable photocatalysis, (solar) energy conversion and light emitting diodes.[1–4] Hence, considerable efforts have been undertaken to explore this compound class in the recent years[5,6] with creative designs utilizing excited states of different characters like metal-to-ligand (MLCT),[7] ligand-to-metal, ligand-to-ligand charge transfer, and metal-centered (MC) states,[8,9] covering zirconium,[10–14] vanadium,[15–18] chromium,[19–26] iron,[27–29] manganese,[30–32] cobalt,[33,34] copper[35–37], molybdenum,[38–42] and zinc as metal centers[43,44] amongst others.

However, elaborate ligand scaffolds are often required to unlock the desired long-lived excited states for photoactivity with earth-abundant metals. While the investigation of these complexes broadens our general understanding of the underlying photophysics, their lengthy syntheses impose a limitation on the sustainability and the overall discovery process of new compounds.[6]

In contrast, complexes of precious metals such as ruthenium(II), iridium(III) or osmium(II) show very favorable optical properties even with simple polypyridyl ligands, $[Ru(bpy)_3]^{2+}$ (bpy = 2,2'-bipyridine) being the prime example.[45–49] However, the high cost and limited abundance of these metals discourage wide-spread applications. As such, photoactive complexes that combine earth-abundant metal centers with simple ligands are highly desirable but generally challenging to design.

Earth-abundant molybdenum(0) shares the $4d^6$ electronic configuration with ruthenium(II), which makes it an attractive substitute for the precious metal ion. Recent studies successfully installed long-lived ^{3}MLCT states in molybdenum(0) complexes using multi-dentate isonitrile ligands. For example, complex **A** (Scheme 1) showed intense green luminescence

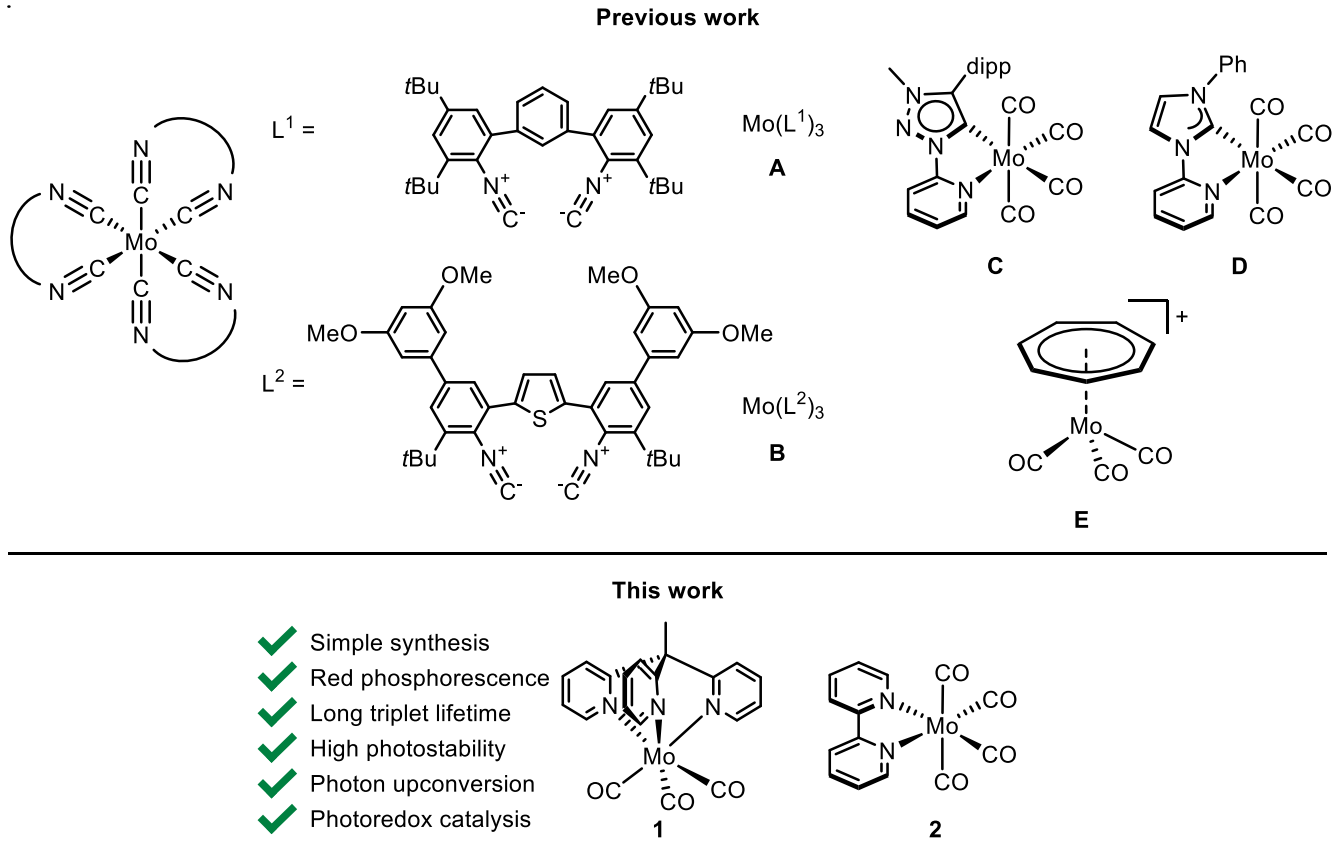

Scheme 1: Structures of representative examples of emissive molybdenum(0) complexes from literature (A–E) and of the compounds investigated in this work (1 and 2).

and also proved to be a strong photoreductant that can drive demanding redox-neutral photocatalytic transformations.[38,50]

The excited state energy could be lowered by ligand modification and the resulting complex **B** (Scheme 1) enabled efficient photon-upconversion.[39,41] However, while these multi-dentate isonitrile complexes possess remarkable properties and provide valuable photophysical insights, they require laborious syntheses of 7–10 steps.[41,50]

In principle, carbonyl ligands in combination with suitable co-ligands present a simple alternative to isonitriles as they show similar bonding properties and their complexes are easily accessible from homoleptic metal precursors $M(CO)_n$.[51] In fact, early studies on molybdenum(0) complexes of the type $Mo(CO)_4$(L^L) with bidentate poly(pyridyl) co-ligands L^L like **2** (Scheme 1) found a weak red phosphorescence from ^{3}MLCT states.[52,53] Similarly, weak red-to-near infrared (NIR) emission was detected from solid complex **C** (Scheme 1) employing a bidentate mesoionic carbene co-ligand.[40,54,55] With a bidentate *N*-heterocyclic carbene co-ligand (complex **D**, Scheme 1) emission in solution was achieved at 681 nm and the complex could be used as a photoredox catalyst.[56] However, high-energy blue light was necessary to drive the catalytic reactions,[56] which likely makes the complex more prone to photodegradation.

A high photostability is generally desirable for photocatalysts and photosensitizers. In this regard, tetracarbonyl complexes with bidentate co-ligands are disadvantageous as their two *trans*-CO ligands are labilized *via* the *trans*-influence, which facilitates dissociation.[57] This situation can be avoided with tripodal co-ligands. However, reports on photoactivity from these systems are scarce with the tropylium complex **E** (Scheme 1) being one of the few examples. **E** shows yellow ^{3}MLCT phosphorescence and undergoes photoreduction in ethanol.[58] Other studies using tripodal tris(pyridyl)-type co-ligands of the type Py_3X with different bridging groups X = CH, P, Al, In and Sn, have so far focused on structural properties and thermal reactivity.[59–63]

To fill this gap, we herein report the photoactive molybdenum(0) tricarbonyl complex **1** (Scheme 1) featuring the tripodal ligand tris(pyridyl)ethane (tpe) and reinvestigate $Mo(bpy)(CO)_4$ **2** for comparison. **1** is available in two steps from commercial staring materials with high overall yield (78 %). The complex exhibits intense deep-red luminescence with excited state lifetimes of several hundred nanoseconds, which is comparable to $[Ru(bpy)_3]^{2+}$ and two orders of magnitude longer than for **2**. Remarkably, **1** shows a higher photostability than the benchmark complex $[Ru(bpy)_3]^{2+}$ under irradiation with green light. Finally, we demonstrate the use of **1** as a sensitizer in green-to-blue photon upconversion with 9,10-diphenylanthracene (DPA) and as a photoreductant in green-light driven photoredox catalysis as a proof-of-principle.

Results and Discussion

Synthesis

The ligand tpe (tpe=1,1,1-tris(pyrid-2-yl)ethane) was synthesized according to a literature procedure from commercially available 2-fluoropyridine and 2-ethylpyridine (78 % yield).[64] The complex $Mo(CO)_3$(tpe) **1** was obtained in quantitative yield as bright red needles by heating commercial $Mo(CO)_6$ and tpe in mesitylene/diglyme in a microwave for 10 min

(Scheme 2, SI, Route A). This procedure guarantees short reaction times and avoids sublimation of $Mo(CO)_6$ that reduces yields when heating under reflux (SI, Route B). The identity of the complex was confirmed by ^1H NMR spectroscopy, mass spectrometry and elemental analysis (see Supporting Information (SI), Figures S1–S2). $Mo(bpy)(CO)_4$ **2** was synthesized according to a published procedure.[53]

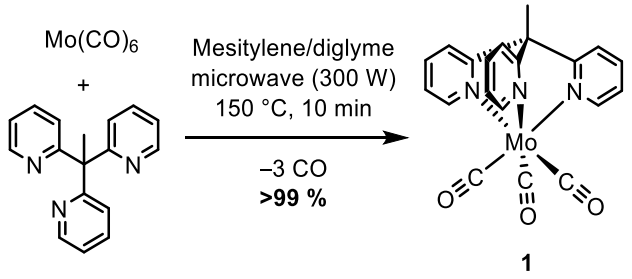

Scheme 2: Synthetic route to 1.

IR Spectroscopy, Crystal Structure, and Redox Chemistry

The facial coordination of the tpe ligand in **1** was confirmed by infrared (IR) spectroscopy. **1** shows two intense absorption bands at 1777 cm^{-1} and 1898 cm^{-1} (Figure S3) that can be assigned to C–O stretching vibrations of *E* and A_1 symmetry in the C_{3v} point group.[65] The IR bands further agree well with literature values for $Mo(CO)_3$(tris(pyrid-2-yl)methane).[59]

The solid-state structure of **1** was elucidated using X-ray diffraction. Single crystals were obtained by recrystallization of **1** from hot DMF. **1** crystallizes in the space group *Cc* (Figure 1, Table S1 in SI). The average Mo–C and Mo–N bond lengths were determined as 1.95 and 2.24 Å, respectively, and agree with an optimized geometry obtained from density functional theory (DFT) calculations (B3LYP/ZORA/TZVP/CPMP(MeCN), see SI, Tables S1 and S2). In the crystal, each molecule shows strong π–π interactions[66] to two of its neighbors (centroid distance *d*=3.652(9) Å, Figure 1b).

For comparison, literature-known **2** features similar Mo–C and Mo–N bond lengths in the solid state, except for the two *trans* Mo–CO bonds which are elongated to 2.04 Å due to the *trans*-influence.[57,67] This is also well reproduced by a DFT-optimized geometry of **2** (Figure S4, Table S3).

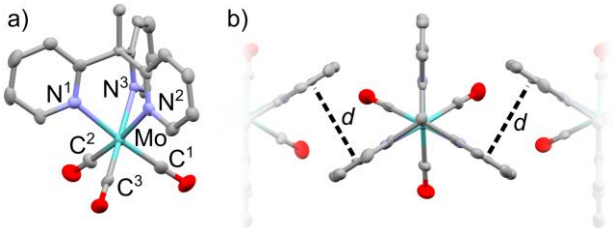

Figure 1. Molecular structure of **1** in the crystal in a) side view and b) top view visualizing the π–π interactions between neighboring molecules with the distance between centroids *d* = 3.652(9) Å. Thermal ellipsoids are displayed at 50 % probability. Hydrogen atoms omitted for clarity.

In solution, **1** shows a reversible and an irreversible oxidation wave with $E_{½}$ = +0.17 to +0.30 V and $E_{p,1}$ = +0.82 to +1.20 V *vs.* SCE depending on the solvent (Table 1, Figures S5–S14). The potential of the reversible oxidation of **1** is thus in between the oxidation waves of **B** (+0.10 V in THF)[41] and **2** (+0.64 V in MeCN, irrev.).[68] The redox events found for **1** are attributed to metal centered oxidations ($Mo^{0/I}$ and $Mo^{I/II}$). The reduction of the pyridine units occurs outside the solvent windows (ca. –1.6 V *vs.* SCE).

Table 1. Electrochemical data of 1, 2 and B with half-wave potentials $E_{½}$ and peak potentials of irreversible waves E_p.

Complex/Solvent	$E_{½}$ / V ($Mo^{0/I}$)	$E_{p,1}$ / V ($Mo^{I/II}$)	$E_{p,2}$ / V	Ref.
1/MeCN	+0.17	+0.82		This work
1/DCM	+0.17	+1.20	+1.36	This work
1/DMF	+0.25	+1.03		This work
1/DMSO	+0.30	+1.01		This work
1/THF	+0.25	+1.04		This work
2/MeCN	+0.64*,[a]	+1.17[a]		68
B/THF	+0.10	–		41

All potentials *vs.* SCE. Electrolyte: 0.1 M [^{n}Bu$_4$N][PF_6] if not stated otherwise. *a* Electrolyte: 0.1 M [^{n}Bu$_4$N][BF_4]. * Peak potential of irreversible wave.

To support this assignment, **1** was oxidized in MeCN with one equivalent of ferrocenium hexafluorophosphate and a UV/Vis absorption spectrum was recorded. The absorption spectrum of $\mathbf{1}^+$ is in excellent agreement with time-dependent DFT (TD-DFT) calculations performed on an optimized geometry of low-spin $[Mo^I(CO)_3(tpe)]^+$ $\mathbf{1}^+$ with an oxidized metal center (Figure S15).

Optical Spectroscopy

UV/Vis absorption spectra of **1** were recorded in several solvents (Figure 2) and molar absorption coefficients of **1** were determined in DMSO, DMF, THF, DCM and MeCN with an uncertainty of 3.5 % (Table 2, see SI for details).

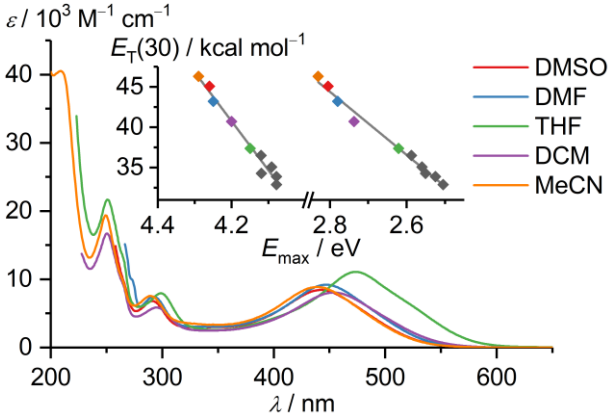

Figure 2. UV/Vis absorption spectra of **1** in various solvents at room temperature. Inset: Empirical solvent polarity parameter $E_T(30)$[69] plotted against energy at the band maxima of the two lowest energy MLCT absorptions; gray lines are linear fits. The dark grey points are taken from absorption spectra in other solvents (Figures S23–S28).

The spectra contain up to four absorption bands at around 450, 300, 250 and 220 nm (Table 2). To assign the transitions, TD-DFT calculations (B3LYP/TZVP/ZORA/CPCM(MeCN)) were performed on an optimized geometry of **1** and analyzed with regards to the different contributions to each transition using the TheoDORE package (Figures S17, S18, S62, S63).[70] The lowest energy absorption around 450 nm is thus assigned to a ^{1}MLCT(Mo+CO→tpe) transition. The contribution of carbonyl ligands is attributed to the strong covalency of the Mo – CO bonds. The two absorption bands at 300 and 250 nm correspond to ^{1}MLCT(Mo→CO) transitions and the high-energy band at 209 nm in MeCN is attributed to ligand-centered ^{1}(π-π*) transitions.

2 absorbs strongly in the blue and UV spectral region in THF and benzene (Table 2, Figures S35 and S36). For **2**, the lowest energy transition at 474 to 494 nm mostly features (Mo+CO)→bpy character (Figure S62), while the Mo→CO transitions are obscured by intense ligand-centered π-π* absorptions (<300 nm).

The ^{1}MLCT absorption bands of **1** and **2** show strong solvatochromic shifts that can be linearly correlated with the empirical solvent polarity parameter $E_T(30)$[69] (see inset in Figure 2, Figure S39). In fact, the solvent sensitiviy of the lowest energy ^{1}MLCT absorption in **1** and **2** is almost identical (Figure S39).[71] Negative solvatochromism indicates a higher polarity of the ground state (GS) compared to the ^{1}MLCT excited state. The GS is stabilized in a more polar solvent environment, which leads to an increased energy of the electronic transition.[72] The Mo→CO bands in **1** are more sensitive to the solvent compared to the (Mo+CO)→tpe absorptions, presumably due to a higher change in dipole moments between ground and excited states in this case.

Table 2: Absorption band maxima λ_{max} and molar absorption coefficients ε of 1 and 2 in different media at room temperature if not stated otherwise, with assignments drawn from charge transfer number analyses[70] of TD-DFT calculations.

	1				
Medium	λ_{max} / nm (ε / 10^3 M^{-1} cm^{-1} *a*)				
	MLCT (Mo→tpe)	MLCT (Mo→CO)			π–π*
MeCN	439 (8.86)	289 (7.55)	264 (9.99)	249 (19.4)	209 (40.5)
DMSO	442 (8.43)	291 (6.85)	266 (9.15)		
DMF	447 (9.20)	293 (7.44)	273 (9.70)		
DCM	454 (8.06)	295 (5.89)	266 (8.94)	250 (16.7)	
THF	473 (11.1)	299 (7.99)	265 (12.9)	251 (21.7)	
2-MeTHF	479	301	266	250	
2,5-Me_2THF	484	303			
Benzene	486	301			
Toluene	491	304			
Xylenes	493				
Mesitylene	495	304			
2-MeTHF (77 K)	451				
KBr Pellet	450*b*				
	2				
Medium	λ_{max} / nm (ε / 10^3 M^{-1} cm^{-1})				
	MLCT (Mo→bpy)			π–π*	π–π*
THF	474 (5.24)	390 (3.88)	348 (4.80)	299 (35.6)	259 (34.8)
Benzene	494 (5.04)	393*c* (3.85)	355 (4.85)	301 (33.1)	

a Experimental uncertainty ±3.5 %. *b* Determined from absorptance measurements of **1** (0.0055 w%) diluted in KBr (Figure S16). *c* Shoulder.

Excitation of **1** in solution with UV/Vis light yields a strong red emission peaking at 720 nm (Figure 3, Table 3) that we assign to a ^{3}MLCT state (see below). Excitation spectra follow the corresponding absorption spectra, which underlines that the emissive lowest excited state is efficiently populated after high-energy excitation (Figures S18–S28).

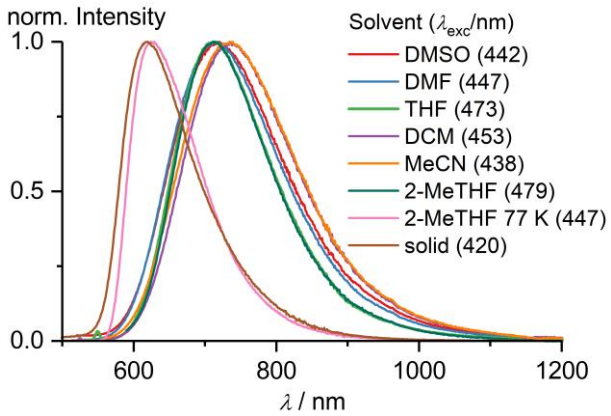

Figure 3: Emission spectra of **1** in various solvents and in the solid state (at 20°C, if not stated otherwise). Emission spectra in other solvents can be found in the SI, Figures S24–S28.

2 shows a single emission band in the NIR at 820 nm in THF and benzene solution (Table 3, Figures S35 and S36). This contradicts an earlier study that reported a dual emission at 578 and 773 nm in benzene solution for **2** and complexes of the type $M(CO)_4(L\wedge L)$ (M = Cr, Mo, W) in general.[52] These results were rationalized with two emissive ^{3}MLCT states with strongly differing excited state distortions. As we were able to fully reproduce the emission band profile of a suitable organic standard dye with our setup (λ_{max} = 700 nm, Figure S40),[73] we propose a single radiative ^{3}MLCT→^{1}GS transition for **2** in solution, instead.

In deaerated solutions, **1** displayed monoexponential luminescence decays with long lifetimes of up to 478 ns depending on the solvent (Table 3, Figure S32) which warrant an assignment as phosphorescence. In contrast, the emission of **2** is only short-lived with very short lifetimes of 0.91 and 1.2 ns in THF

and benzene solution, respectively (Table 3, Figures S37 and S38).

In the solid state, the luminescence decay of **1** was fitted with three exponential functions with an amplitude averaged lifetime of 78 ns (Table 3, Figure S33).

According to DFT calculations (B3LYP/TZVP/CPCM(MeCN), see SI for details), the emissive lowest excited state in **1** is best described as a ^{3}MLCT state with the radical anion localized on one pyridyl moiety (Figure S64–S65). In its fully relaxed geometry, the ^{3}MLCT state is predicted at an energy of 2.01 eV (616 nm) relative to the ^{1}GS. It features a geometry with elongated Mo^I–CO bonds (two bonds +0.04 Å, one bond +0.09 Å) due to the reduced π-backbonding and a contracted Mo^I–N_{py} bond to the pyridyl radical anion (–0.10 Å) due to the Coulomb attraction. The emission energy was calculated as the energy difference between the relaxed ^{3}MLCT state and the ^{1}GS with ^{3}MLCT geometry (Franck-Condon point for emission, Figure S64) as 1.67 eV and is in excellent agreement with the emission band maximum in MeCN at 1.69 eV (735 nm, Table 3, Figure 3). A second excited state of ^{3}MC character ($t_{2g} \rightarrow e_g$ excitation) is located at 2.17 eV (572 nm) above the ^{1}GS. The large contribution of Mo–CO orbitals results in a bent CO coordination with an ∠(Mo–C–O) angle of 135° (Figure S65) suggesting a high covalency of the Mo–CO bond. In **2**, two Mo–CO bonds are already elongated in the ^{1}GS due to the *trans* influence (+0.07 Å). The ^{3}MLCT state energy of **2** (1.87 eV) is lower than for **1** because the spin density is delocalized over the bpy ligand (Figure S65). The two Mo–CO bonds *trans* to the $(bpy^{\bullet})^-$ are elongated (+0.09 Å). The ^{3}MC state of **2** (2.20 eV) features two bent Mo–CO bonds (166°). The energies of high-spin ^{5}MC states were calculated at 4.07 and 4.14 eV for **1** and **2**, respectively, which makes them irrelevant for the photophysics following low-energy ^{1}MLCT excitation (Table S10).

In solution, **1** showed a high phosphorescence quantum yield Φ with 1.2 % being the highest value obtained in deaerated toluene (Table 3). The quantum yields decreased with increasing polarity of the solvent (Figure S31) reaching 0.13 % in MeCN (Table 3). To the best of our knowledge, the phosphorescence lifetimes and quantum yields of **1** are the highest measured for zero-valent molybdenum carbonyl complexes so far[40,52,74] and are comparable to those of **B** (Φ = 1.5 %, τ = 56 ns in deaerated toluene).[41] In contrast, the quantum yields of **2** in THF and benzene were found to be very low (≈0.01 %, Table 3).

Table 3: Luminescence data of 1 and 2 in various media with emission maximum λ_{em}, emission lifetime τ, emission quantum yield Φ and radiative rate $k_r = \Phi/\tau$.

Complex	Medium	λ_{em} /nm	τ/ns [a]	Φ/% [a]	k_r /10^4 s^{-1} [a]
1	MeCN	735	127	0.13[b]	1.0
1	d_3-MeCN		134		
1	DMSO	719	184	0.23[b]	1.3
1	DMF	715	215	0.26[b]	1.2
1	DCM	735	146	0.45[b]	3.1
1	THF	715	355[c]	0.66[b]	1.9
1	d_8-THF		378		
1	2-MeTHF	712	412	0.79[b]	1.9
1	2,5-Me_2THF	712	460	0.91[d]	2.2
1	Benzene	718	411	1.2[d]	2.9
1	Toluene	712	457	1.2[d]	2.6
1	Xylene	716	478	1.0[d]	2.1
1	Mesitylene	717	471	1.0[d]	2.1
1	2-MeTHF (77 K)	625	27600	–	–
1	2-MeTHF (143 K)	712	2900		
1	Solid	616	78[e]	1.0[b]	13
1	Solid (77 K)	634	–	14[b]	–
1	KBr Pellet	650	200[f,h]	–	–
1	KBr Pellet (5 K)	647	29000[g,h]	–	–
2	THF	820	0.91	0.009[b,h]	9.9[h]
2	Benzene	820	1.2	0.012[b,h]	10[h]

a Estimated error: ±5 %. *b* Absolute values determined using an integrating sphere setup. *c* The lifetime in THF is unaffected by the presence of the stabilizer dibutylhydroxytoluene (BHT). *d* Determined relative to $[Ru(bpy)_3]Cl_2$ in aerated water (see SI for details). *e* Amplitude weighted average lifetime obtained from a triexponential fit with τ_1 = 22 ns (18 %), τ_2 = 110 ns (45 %), τ_3 = 442 ns (37 %). *f* Amplitude weighted average lifetime obtained from a biexponential fit with τ_1 = 190 ns (99.8 %), τ_2 = 760 ns (0.2 %). *g* Amplitude weighted average lifetime obtained from a biexponential fit with τ_1 = 5200 ns (28 %), τ_2 = 39000 ns (72 %). *h* Estimated error: ±10 %.

Upon cooling of a solution of **1** in 2-MeTHF to 77 K, the ^{1}MLCT(Mo+CO→tpe) absorption band is blue-shifted from 479 to 451 nm (+1300 cm^{-1}, Figure S23). Similarly, the emission band shifts from 712 to 628 nm (+1900 cm^{-1}) and sharpens (Figure S23). This pronounced shift is known as rigidochromism and commonly observed for MLCT states in carbonyl complexes.[75,76] The spectral changes are not caused by the lower temperature but the rigidity of the environment as demonstrated by the similarity of the emission bands of solid **1** at room temperature and **1** in frozen 2-MeTHF solution at 77 K (Figure 3). Conversely, the emission maximum in a KBr pellet did not shift significantly upon cooling to 5 K, while the integrated emission intensity rose by approximately one order of magnitude (Figure S41). In both the KBr pellet at 5 K and in frozen solution at 77 K the emission lifetime increased dramatically to 29 and 27.6 µs, respectively (Figures S34, S41–S43, Table S4), which hints to a thermally activated non-radiative decay pathway. An impressive luminescence quantum yield of 14 % was determined for solid **1** at 77 K.

The typical deactivation pathway in d^6 ^{3}MLCT emitters is thermally-activated non-radiative relaxation via the ^{3}MC states.[41,77,78] To investigate this path, we measured the phosphorescence lifetimes of **1** in MeCN, THF and benzene at different temperatures (Figure S44). The luminescence lifetimes decreased with increasing temperatures due to facilitated thermal population of the detrimental ^{3}MC state. A simple but well-established three parameter model[41,79,80] was used to fit the data (Figure S44, Table S5). This approach yielded an energy difference ΔE of 1600 cm^{-1} for the ^{3}MLCT–^{3}MC interconversion in **1** in all three solvents, which is in excellent

agreement with the calculated energy of 1400 cm^{-1} of a DFT-optimized ^{3}MLCT–^{3}MC transition state (Figure S64).

While the DFT-calculated energy gap between ^{3}MLCT and ^{3}MC states in **2** (2600 cm^{-1}) is larger than in **1** (Figure S64), the excited state lifetimes of **2** are two orders of magnitude shorter. One reason is the faster deactivation of excited states with lower energy (energy gap law). Additionally, the labilized *trans*-CO bonds in **2** might enable deactivation pathways with low energy barriers.

Time-Resolved Spectroscopy

To further investigate the long-lived excited state in **1**, transient absorption (TA) spectra were recorded using laser flash photolysis 532 nm pulses of ~10 ns duration in THF (black trace in Figure 4a). The ns-TA spectrum was calibrated using the TA signal of an isoabsorptive $[Ru(bpy)_3]Cl_2$ solution in water and its difference molar absorption coefficient $\Delta\varepsilon$(455 nm) = –10100 M^{-1} cm^{-1} (see SI for details, Figure S45 and S46).[81–83]

After pulsed laser excitation, **1** shows an intense ground state bleach at 476 nm ($\Delta\varepsilon$ = –8400 M^{-1} cm^{-1}) and four excited state absorption bands (235, 328, 375, 700 nm, see Figure 4a) in THF. All TA bands decay monoexponentially with a time constant of (354±3) ns (Figure 4b), that perfectly matches the luminescence lifetime of **1** in THF (355 ns, Table 2). Using femtosecond laser pulses at 480 nm, ultrafast dynamics like the ^{1}MLCT→^{3}MLCT intersystem crossing (ISC) or vibrational cooling could not be resolved (Figure S49) and can therefore be considered faster than the time resolution of the experiment (0.5 ps), similar to the fast and efficient ISC in $[Ru(bpy)_3]^{2+}$.[84,85]

By adding the steady state absorption spectrum in THF (Figure 2) to the calibrated TA spectrum (Figure 4a) we isolated the pure absorption spectrum of the long-lived excited state of **1** (Figure 4c). The excited state features five absorption bands (Table S6) that match very well with the TDDFT calculated oscillator strengths of the optimized ^{3}MLCT state – supporting the previous assignment of the excited state character. The nature of the electronic transitions in the ^{3}MLCT state was further elucidated using a charge transfer number analysis[70] (Figure 4c and Table S6). Compared to the ^{1}GS, the ^{3}MLCT transitions (Mo^I→py_2; py_2 = unreduced part of the tpe ligand) in the ^{3}MLCT state of **1** are blue-shifted with a band maximum at 375 nm. This is expected considering the lower electron density at the formally oxidized Mo^I center. Additional lower energy bands arise from transitions involving the ligand-centered radical-anion $py^\bullet$ (*i.e.* LMCT, LL'CT and LC($py^\bullet$) transitions).

In addition to UV-visible spectroscopy, the intense C=O stretching vibrations in carbonyl complexes present excellent probes for excited states. To confirm that the long-lived excited state in **1** is a ^{3}MLCT state, we recorded ns-step-scan FTIR spectra in d_6-DMSO and in a KBr pellet (Figures S50–S56). In the ^{1}GS, **1** shows two intense IR absorption bands of the C–O stretching vibrations at 1777 cm^{-1} and 1898 cm^{-1} (*E* and A_1 in C_{3v} symmetry) in DMSO. After pulsed excitation at 532 nm, a GS bleach as well as three new absorption bands (1829, 1870, 1975 cm^{-1}) emerge. The splitting of the *E* band confirms the reduction in symmetry in the excited state. All IR features decay with a common time constant of 150 ns (Figure S55) that is consistent with the emission lifetime of 184 ns (Table 3). The excited state IR spectrum (Figure S56) can be reasonably described by DFT calculations of **1** in a relaxed ^{3}MLCT geometry with CO bands at 1850, 1881 and 2012 cm^{-1}, confirming the experimental hypsochromic shifts and the splitting of the *E* band. This supports the ^{3}MLCT assignment of the long-lived excited state. In an ultrafast fs-Vis-pump-IR-probe experiment, the ^{3}MLCT bands already appear 1 ps after photoexcitation confirming the population of the long-lived ^{3}MLCT state via rapid ISC (see SI for details, Figures S57–S59). This also confirms the data from Vis/NIR-fs-TA spectroscopy.

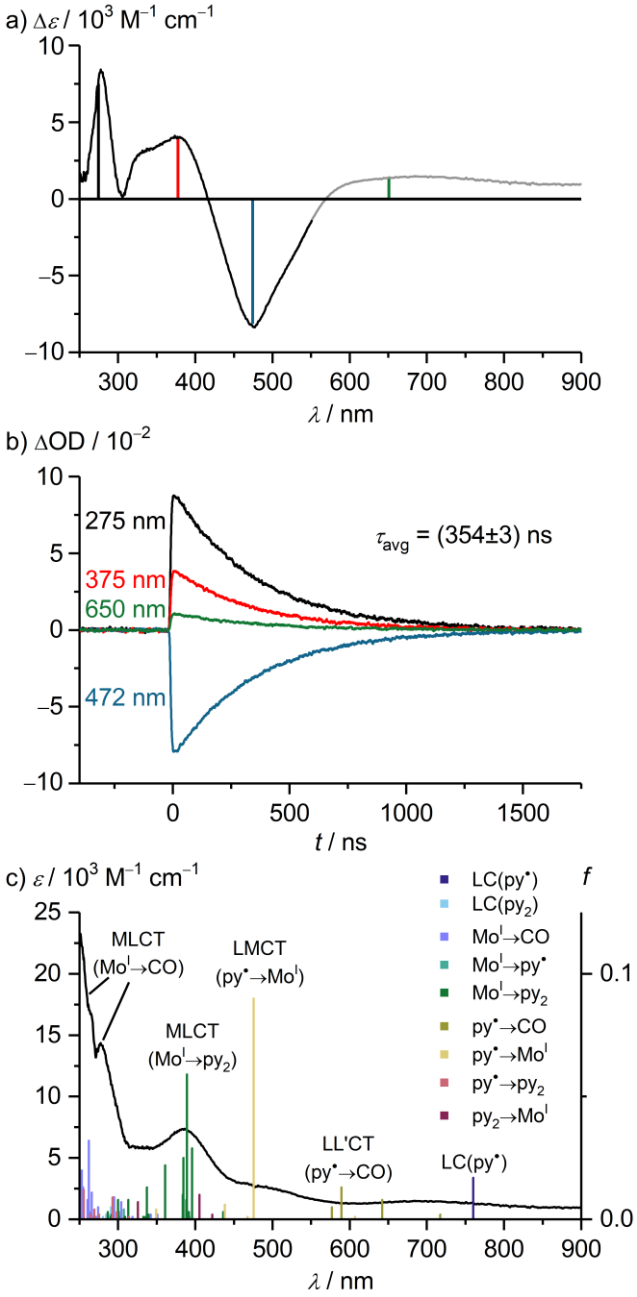

Figure 4. Transient absorption studies on **1** in deaerated THF at 20 °C. a) UV/Vis-ns-TA spectrum (black line, λ_{exc} = 532 nm, delay: 10 ns, integration time: 110 ns) calibrated using $[Ru(bpy)_3]Cl_2$ in water as a reference (see SI for details), and Vis/NIR-fs-TA spectrum (gray line, λ_{exc} = 480 nm, integration time: 7.8 ns) scaled to fit to the calibrated spectrum at 532 nm. b) Kinetic traces of the ns-TA at selected wavelengths. c) Absorption spectrum of the ^{3}MLCT state of **1** in THF (see

main text for details). The sticks represent oscillator strengths *f* of the DFT-optimized ^{3}MLCT state calculated using TDDFT (B3LYP/TZVP/CPCM(THF), simulated spectrum: Figure S47). The colors of the sticks indicate the dominant character of the transition derived from a charge transfer number[70] analysis ($py^\bullet$ = pyridine centered radical anion, py_2 = unreduced part of the tpe ligand).

Stability

Transition metal carbonyl complexes are well-known for their thermal and photochemical decarbonylation reactions which is exploited in CO-releasing molecules for therapeutic treatments.[86] However, for other light-driven applications like photon upconversion or photocatalysis a high photostability is desirable.

When stored in the dark, a solution of **1** in deaerated THF is stable at room temperature as demonstrated by the long half-life of 158 d determined by UV/Vis absorption spectroscopy (Figure S60).

To probe the photostability of **1** and **2**, we irradiated isoabsorptive solutions (A = 0.16) of the complexes in THF with a green cw-laser (514 nm, 827 mW, 20 °C). For comparison we also measured the photodegradation of $[Ru(bpy)_3][PF_6]_2$ in MeCN. During irradiation, we monitored the luminescence intensity, which we assume to be proportional to the concentration of the complexes (Figure S61, Table S9). We obtained the absolute photodegradation quantum yields Φ_{degr} from the experimental parameters according to a published procedure (see SI for details).[87]

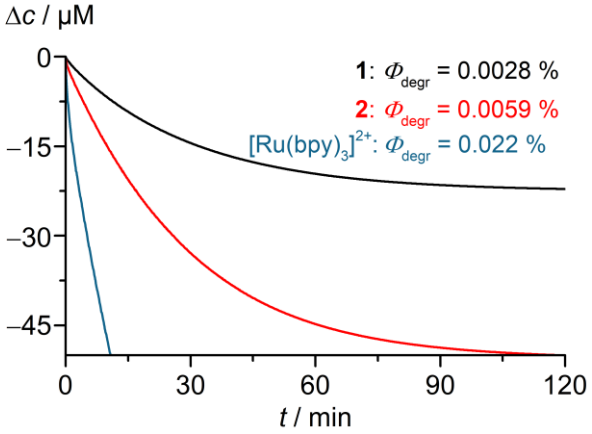

Figure 5. Photostability of **1** (black trace) and **2** (red trace) in deaerated THF, and $[Ru(bpy)_3][PF_6]_3$ in deaerated MeCN (blue trace) under irradiation with a green cw-laser (λ_{exc} = 514 nm, P = 827 mW) at 20°C with the photodegradation quantum yield Φ_{degr}. The concentration changes Δc were derived from photoluminescence measurements (see SI for details, Figure S61, Table S9).

This method yielded photodegradation quantum yields Φ_{degr} of 0.0028 % for **1**, 0.0059 % for **2** and 0.022 % for $[Ru(bpy)_3][PF_6]_2$. The values for **2** and the ruthenium complex are in line with previous literature reports.[52,87] Interestingly, **1** appears to be one order of magnitude more photostable than $[Ru(bpy)_3]^{2+}$. The photodegradation quantum yield of **2** is twice as high as that of **1**, which is attributed to the *trans*-Mo–CO bonds in **2** that labilize each other as they compete for the same *d*-orbitals which weakens their π-backbonding (*trans* influence).[57] The difference in photostability becomes more apparent when comparing dissociation rate constants that can be estimated using $k_{degr} = \Phi_{degr}/\tau$ and take the excited state lifetime τ into account: While decomposition of **2** is very fast with k_{degr} = 65,000 s^{-1}, **1** decomposes almost three orders of magnitude slower with a time constant of 79 s^{-1}. Hence, avoiding *trans*-CO bonds is a useful strategy to significantly increase photostability.

The interpretation given above is supported by DFT optimized geometries of **1** and **2** in their respective ground and excited states. In general, the shortest Mo–CO bonds are obtained when the carbonyl ligand is *trans* to a pyridyl ligand (ca. 1.96 Å) and elongated by *ca.* 0.1 Å when *trans* to another Mo–CO ligand or to a pyridyl radical anion in the ^{3}MLCT state (Table S10). There are no *trans*-CO ligands in **1** and its ^{3}MLCT state is localized on a single pyridyl moiety ($py^\bullet$). Hence only one Mo–CO bond is significantly elongated in the ^{3}MLCT state of **1**. In contrast, **2** already features two *trans*-CO ligands in the GS and the radical anion in the ^{3}MLCT state is delocalized on both pyridyl units of the bpy ligand (Figure S65). Consequently, all four Mo–CO bonds in **2**'s ^{3}MLCT state are elongated, decreasing the photostability of the ^{3}MLCT state.

DFT-calculated potential energy wells of **1** reveal high barriers for CO dissociation in the ^{1}GS (20700 cm^{-1}), ^{3}MLCT (17600 cm^{-1}) and ^{3}MC states (7400 cm^{-1}) in line with the experimentally observed stability of this complex (Figure S66). For **2**, these barriers are significantly lower for both types of CO ligands (*trans* to a pyridyl moiety and *trans* to another CO ligand, Figures S67, S68, Table S11) in all three electronic states we investigated (^{1}GS, ^{3}MLCT, ^{3}MC). Interestingly, **2** shows particularly weak bonds of the two CO ligands *trans* to each other in the ^{3}MLCT state with a low dissociation energy of 6700 cm^{-1}. This is due to the weaker back-bonding of the CO ligands to the formally oxidized metal center Mo^I and the lack of stabilization by a *trans* $(bpy)^{\bullet-}$ ligand. Hence, (reversible) CO dissociation[54] likely presents an additional deactivation pathway for the ^{3}MLCT state in **2** that is unavailable in **1** and further helps to explain the higher excited state lifetimes and photostability of **1**.

Photon Upconversion

As a first application of the long-lived ^{3}MLCT excited state of **1**, we explored sensitized triplet-triplet annihilation (sTTA) upconversion (UC). In sTTA-UC processes, the energy of a sensitizer's triplet state is transferred to a suitable (organic) acceptor via a Dexter energy transfer (k_{TTET}). Upon collision of two acceptors in their triplet states the triplets can annihilate (TTA), which returns one acceptor to its GS and raises the other one to a high-energy singlet state. This singlet state can then show delayed anti-Stokes shifted fluorescence and hence is called upconverted emission.[1,88,89]

As an acceptor we chose DPA, which dynamically quenches the ^{3}MLCT state of **1** at a nearly diffusion limited rate of k_{TTET} = $1.5 \cdot 10^9$ M^{-1} s^{-1} in THF at 20°C (Figure S69 and S70). This is almost one order of magnitude faster than the quenching of **B** with DPA,[41] which we attribute to the better orbital overlap between excited **1** and DPA due to the more compact ligand design and less steric shielding in **1**.

The formation of ^{3}DPA from photoexcited **1** (**1***, ^{3}MLCT state) was confirmed by transient absorption spectroscopy following laser flash photolysis. The build-up of ^{3}DPA mirrors the decay of the ^{3}MLCT emission of **1** (Figure S71a). After

full decay of the ^{3}MLCT state (ca. 1 µs), ^{3}DPA was detected via its characteristic transient absorption band at 445 nm (Figure S71b).[90,91] The decay of the ^{3}DPA absorption signal was fitted using a previously reported model that considers the mixed first-order (k_{nr}) and second-order (k_{TTA}) deactivation processes (Figure S72).[92]

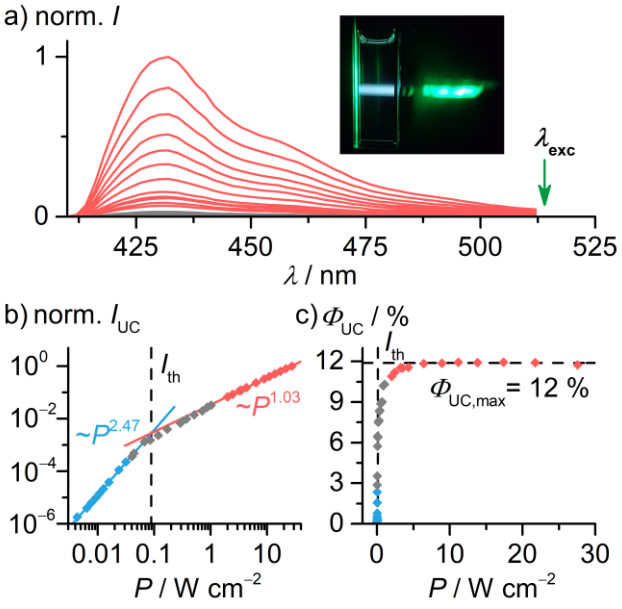

Figure 6. Photon upconversion experiments using **1** in THF in the presence of 10 mM DPA and excitation at 514 nm with a cw-laser (OD_{514} = 0.10, laser spot size: 3 mm^2). a) Spectra of the upconverted DPA fluorescence at different laser power densities *P*. Inset: photograph of the green excitation light and blue upconverted emission. b) Doubly logarithmic plot of the integrated upconverted fluorescence intensity I_{UC} *vs.* laser power density *P*. I_{th} is the threshold intensity. c) Relative upconversion quantum yield Φ_{UC} *vs.* laser power density *P*.

The upconverted ^{1}DPA emission at 435 nm was detected after excitation of a solution of **1** and DPA (10 mM) in THF at 514 nm (Figure 6a). The reduced lifetime of 55 ns revealed a quenching efficiency of 85 %. The DPA concentration of 10 mM was chosen as it marked the sweet spot between efficient quenching and detrimental reabsorption of the DPA fluorescence (Figure S73). In accordance with a two-photon process of the proposed TTA-UC mechanism, we found a quadratic increase of the emission intensity at low excitation power densities, which changed to a linear dependence above the threshold intensity of 0.09 W cm^{-2} (Figure 6b). The UC quantum yield Φ_{UC} reaches a plateau value of 12 % (max. 50 %) at high laser power densities (Figure 6c, see SI for details). No UC emission was found without the sensitizer **1** or without DPA (Figure S74). The photon-UC is also operative with excitation using a green LED (525 nm, Kessil lamp) highlighting the viability of the UC system even at very low power densities (Figure S74).

Photoredox Catalysis

The promising redox and optical properties of **1** with its long-lived ^{3}MLCT state outlined above motivated us to explore the photocatalytic capabilities of this complex as a proof-of-principle.

The energy of the ^{3}MLCT state E_{00} is estimated to 1.85 eV from low-temperature emission spectra and quenching experiments in MeCN (see SI for details). The excited state reduction potential can be calculated using Eq. 1 (Coulomb term omitted) as –1.68 V *vs.* SCE, suggesting a strong photoreducing power of **1**.

$$E(\mathbf{1}^+/\mathbf{1}^*) = E(\mathbf{1}^+/\mathbf{1}) - E_{00} \qquad \text{(Eq. 1)}$$

As a test reaction, we selected the dehalogenation of chloropyrazine, which can also be performed by the one-electron reduced form of $[Ru(bpy)_3]^{2+}$ ($E([Ru(bpy)_3]^{2+/+})$ = –1.29 V *vs.* SCE).[93] In fact, the luminescence of **1** in MeCN is quenched by the substrate with a rate constant k_q of $3.9 \cdot 10^8$ M^{-1} s^{-1} (Figure S75). The triplet energy of chloropyrazine is expected to be ≫2.5 eV[91] and thus way above the estimated ^{3}MLCT energy of **1** (1.85 eV). Hence, triplet-triplet energy transfer can be excluded as a quenching mechanism, leaving photoelectron transfer as the most plausible alternative. The photoredox reaction with the substrate produces $\mathbf{1}^+$ that needs to be reduced by a sacrificial donor to regenerate the catalyst **1**. The high potential for the $\mathbf{1}/\mathbf{1}^+$ couple at +0.17 V *vs.* SCE in MeCN requires a strong reductant for this step. We chose the previously reported benzimidazoline derivative BIH (Scheme 3) for which a suitable reduction potential of +0.13 V *vs.* SCE has been reported in THF.[94] The oxidized donor $BIH^{\bullet+}$ can undergo a second oxidation after deprotonation to $BI^{\bullet}$ with a potential of –1.7 V *vs.* SCE.[94,95] On a side note, the final product BI^+ can be recycled to resynthesize the donor BIH.[94] We confirmed that BIH is able to regenerate **1** from $\mathbf{1}^+$ in MeCN prepared by chemical oxidation (Figure S76) and does not quench the ^{3}MLCT state of **1**.

After we have assessed the required elementary steps of a potential catalytic cycle, we attempted the dehalogenation of chloropyrazine employing 1 mol% **1** in MeCN, 1 eq. BIH and a green LED as an excitation source at 20.0°C (Scheme 3a, Table S12). Yields and conversions were determined using ^{1}H NMR spectroscopy with mesitylene as an internal standard. Under these conditions we obtained pyrazine in a yield of 80 % after 24 h. Control experiments confirmed that catalyst, sacrificial donor and light were necessary for the reaction to occur (Table S12, entries 2–4).

Based on our results we propose the mechanism in Scheme 3b. After photoexcitation of **1** and ultrafast ISC to the ^{3}MLCT state (**1***) the complex reduces the substrate. The one-electron reduced substrate dissociates into a pyrazyl σ-radical and a chloride ion. The product forms via H-atom transfer from BIH to the σ-radical. Meanwhile, BIH reduces the oxidized catalyst $\mathbf{1}^+$ forming **1** and $BIH^{\bullet+}$. The latter radical cation can be deprotonated by a base such as BIH or the pyrazine to the radical $BI^{\bullet}$, which can in turn reduce the substrate and $\mathbf{1}^+$. Since the photocatalytic conversion to the product is rather slow, we conclude that a conceivable photoinitiated radical chain mechanism only plays a minor role (Scheme S1).

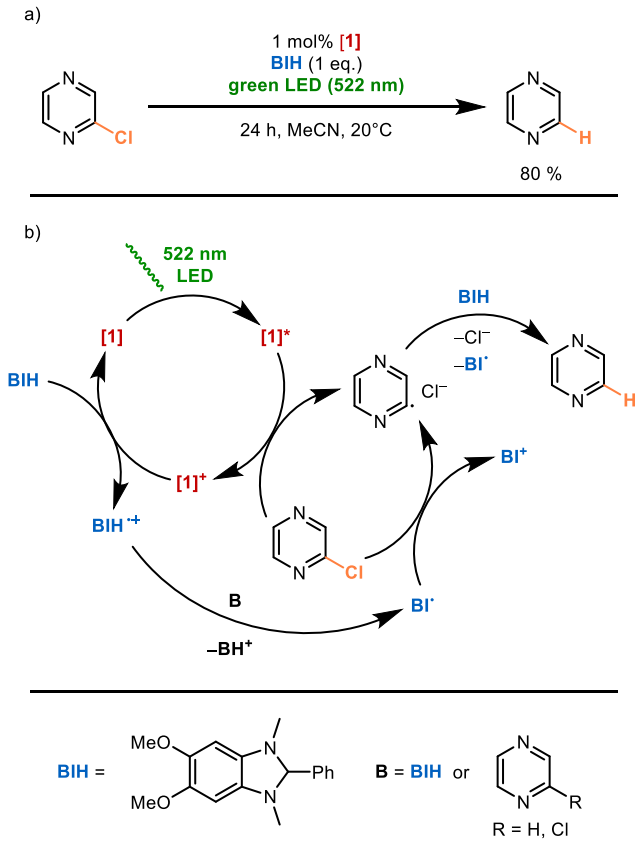

Scheme 3. Application of 1 in photoredox catalysis. a) Overview of the reaction conditions. b) Proposed mechanism for the dehalogenation of chloropyrazine with 1 in green light driven photoredox catalysis.

Conclusions

By combining the tripodal tris(pyridyl)ethane (tpe) with carbonyl ligands we obtained a simple photoactive molybdenum(0) complex $Mo(CO)_3$(tpe) that emits deep-red phosphorescence at 720 nm with a lifetime of up to *ca.* 500 ns in solution at room temperature.

Time-resolved electronic and vibrational spectroscopy in combination with DFT/TD-DFT calculations showed that the emissive state is of ^{3}MLCT character populated after ultrafast ISC. Thermal deactivation occurs *via* a distorted ^{3}MC state with a barrier of 1600 cm^{-1} as revealed by temperature dependent luminescence and DFT calculations. This ^{3}MC state possesses a bent CO ligand instead of a strongly weakened linearly coordinated CO ligand, which would be prone to dissociation. The complex is very photostable under irradiation with a green laser with a photodecomposition quantum yield of merely 0.0028 %. This is one order of magnitude lower than that of $[Ru(bpy)_3]^{2+}$. Compared to $Mo(bpy)(CO)_4$, the estimated rate constant for photodegradation of the tripodal complex is almost three orders of magnitude lower. We attribute this gain in stability to the lack of *trans*-CO bonds in the facial ligand configuration, which avoids additional Mo–C bond elongation in ground and excited states.

DFT calculations on $Mo(CO)_3$(tpe) match experimental data exceptionally well, including the energies of CO stretching vibrations and absorption spectra of the ground and ^{3}MLCT states, the ^{3}MLCT–^{3}MC energy barrier and emission energy.

The new complex served as a sensitizer in green-to-blue photon upconversion with DPA and achieved a high upconversion quantum efficiency of 12 % (max. 50 %). Even a cheap low-power LED sufficed to drive the upconversion process. $Mo(CO)_3$(tpe) successfully acts as a photoredox catalyst in the dehalogenation of 2-chloropyrazine using a recyclable benzimidazoline[94] derivative as sacrificial donor.

Despite the rich literature on carbonyl complexes,[40,52 – 56,71,96,97] their facial coordination with tripodal ligands remained underexplored for photochemical applications so far. Following this promising design strategy, our results delineate how to access photoactive complexes while avoiding precious metals and elaborate ligand syntheses alike. In addition, the exceptional agreement of measured and calculated properties allows for the *in silico* exploration of the chemical space to predict promising synthetic targets. Overall, we hope that this study can guide future research towards more sustainable photochemistry.

ASSOCIATED CONTENT

Supporting Information. CCDC 2251140 contains the supplementary crystallographic data for this paper. These data can be obtained free of charge from The Cambridge Crystallographic Data Centre via www.ccdc.cam.ac.uk/structures. General methods, synthetic procedures, spectroscopic data (NMR, FTIR, UV/Vis absorption, luminescence, transient absorption, step-scan FTIR, fs-Vis-pump-IR-probe spectroscopy), electrochemical data, details of the stability measurements, photon upconversion and photoredox catalysis, DFT-optimized structures. This material is available free of charge via the Internet at http://pubs.acs.org.

AUTHOR INFORMATION

Corresponding Author

* Prof. Dr. Katja Heinze, Department of Chemistry, Johannes Gutenberg University of Mainz, Duesbergweg 10–14, 55128 Mainz, Germany; E-Mail: katja.heinze@uni-mainz.de.

Author Contributions

WRK performed the syntheses, spectroscopic characterization (IR, absorption, luminescence), electrochemical analysis, photostability and photocatalysis experiments, quantum chemical calculations, assisted in upconversion and TA experiments, and wrote the manuscript. MSB and CK performed upconversion and TA experiments, analysed the data and contributed to several discussions related to the whole manuscript. PB performed step-scan IR experiments and temperature dependent luminescence spectroscopy of **1** in the KBr pellet supervised by GNS. ACF optimized the synthesis and crystallization of **1**. RK performed the ICP-MS analysis supervised by NHB. JS and JH performed fs-time-resolved Vis-pump IR-probe experiments and analyzed the data. RN performed fs-TA experiments and analyzed the data. CF solved the crystal structure of **1**. KH supervised the entire study. The manuscript was written through contributions of all authors. All authors have given approval to the final version of the manuscript.

Funding Sources

Max-Planck Graduate Center with the Johannes Gutenberg University (MPGC). Deutsche Forschungsgemeinschaft (DFG) through grants INST 247/1018-1 FUGG to KH and KE 2313/3-1 to CK.

ACKNOWLEDGMENT

The authors thank Dr. Charusheela Ramanan and Prof. Dr. Paul Blom (Max Planck Institute for Polymer Research) for providing access to the fs-TA spectrometer, Naz Uğur (Max Planck Institute for Polymer Research) for valuable experimental support during the fs-TA measurements, Jun.-Prof. Dr. Cui Wang (University of Osnabrück) for preliminary luminescence lifetime measurements, Dr. Luca Carrella for collecting the XRD data, Dr. Johannes Liermann for support with NMR spectroscopic experiments, Dimitri Zorn for support of the synthesis of the sacrificial donor and Lukas Sorge for helpful discussions. W.R.K. is thankful for support by the German Academic Scholarship Foundation (Studienstiftung des Deutschen Volkes) and for financial support by the Max-Planck Graduate Center with the Johannes Gutenberg University (MPGC). C.K. and M.-S.B. are grateful to the Chemical Industry Funds for financial support. Parts of this research were conducted using the super-computer Elwetritsch and advisory services offered by the University of Kaiserslautern-Landau (https://hpc.rz.rptu.de), which is a member of the AHRP and the Gauss Alliance e.V.

REFERENCES

(1) Schloemer, T.; Narayanan, P.; Zhou, Q.; Belliveau, E.; Seitz, M.; Congreve, D. N. Nanoengineering Triplet-Triplet Annihilation Upconversion: From Materials to Real-World Applications. *ACS nano* **2023.** DOI: 10.1021/acsnano.3c00543.

(2) Larsen, C. B.; Wenger, O. S. Photoredox Catalysis with Metal Complexes Made from Earth-Abundant Elements. *Chem. Eur. J.* **2018**, *24* (9), 2039 – 2058. DOI: 10.1002/chem.201703602.

(3) Förster, C.; Heinze, K. Photophysics and photochemistry with Earth-abundant metals - fundamentals and concepts. *Chem. Soc. Rev.* **2020**, *49* (4), 1057 – 1070. DOI: 10.1039/C9CS00573K.

(4) Dorn, M.; East, N. R.; Förster, C.; Kitzmann, W. R.; Moll, J.; Reichenauer, F.; Reuter, T.; Stein, L.; Heinze, K. d-d and charge transfer photochemistry of 3d metal complexes. In *Comprehensive Inorganic Chemistry III*; Elsevier, 2023; pp 707 – 788. DOI: 10.1016/B978-0-12-823144-9.00063-7.

(5) Wegeberg, C.; Wenger, O. S. Luminescent First-Row Transition Metal Complexes. *JACS Au* **2021**, *1* (11), 1860 – 1876. DOI: 10.1021/jacsau.1c00353.

(6) Sinha, N.; Wenger, O. S. Photoactive Metal-to-Ligand Charge Transfer Excited States in 3d6 Complexes with Cr0, MnI, FeII, and CoIII. *J. Am. Chem. Soc.* **2023**, *145* (9), 4903 – 4920. DOI: 10.1021/jacs.2c13432.

(7) Kitzmann, W. R.; Heinze, K. Charge-Transfer and Spin-Flip States: Thriving as Complements. *Angew. Chem. Int. Ed.* **2022**, e202213207. DOI: 10.1002/anie.202213207.

(8) Kitzmann, W. R.; Moll, J.; Heinze, K. Spin-flip luminescence. *Photochem. Photobiol. Sci.* **2022.** DOI: 10.1007/s43630-022-00186-3.

(9) Förster, C.; Heinze, K. Bimolecular reactivity of 3d metal-centered excited states (Cr, Mn, Fe, Co). *Chem. Phys. Rev.* **2022**, *3* (4), 41302. DOI: 10.1063/5.0112531.

(10) Zhang, Y.; Petersen, J. L.; Milsmann, C. A Luminescent Zirconium(IV) Complex as a Molecular Photosensitizer for Visible Light Photoredox Catalysis. *J. Am. Chem. Soc.* **2016**, *138* (40), 13115 – 13118. DOI: 10.1021/jacs.6b05934.

(11) Zhang, Y.; Lee, T. S.; Petersen, J. L.; Milsmann, C. A Zirconium Photosensitizer with a Long-Lived Excited State: Mechanistic Insight into Photoinduced Single-Electron Transfer. *J. Am. Chem. Soc.* **2018**, *140* (18), 5934 – 5947. DOI: 10.1021/jacs.8b00742.

(12) Zhang, Y.; Lee, T. S.; Favale, J. M.; Leary, D. C.; Petersen, J. L.; Scholes, G. D.; Castellano, F. N.; Milsmann, C. Delayed fluorescence from a zirconium(IV) photosensitizer with ligand-to-metal charge-transfer excited states. *Nat. Chem.* **2020**, *12* (4), 345 – 352. DOI: 10.1038/s41557-020-0430-7.

(13) Yang, M.; Sheykhi, S.; Zhang, Y.; Milsmann, C.; Castellano, F. N. Low power threshold photochemical upconversion using a zirconium(iv) LMCT photosensitizer. *Chem. Sci.* **2021**, *12* (26), 9069 – 9077. DOI: 10.1039/d1sc01662h.

(14) Leary, D. C.; Martinez, J. C.; Akhmedov, N. G.; Petersen, J. L.; Milsmann, C. Long-lived photoluminescence from an eight-coordinate zirconium(IV) complex with four 2-(2'-pyridyl)pyrrolide ligands. *Chem. Commun.* **2022**, *58* (85), 11917 – 11920. DOI: 10.1039/D2CC04912K.

(15) Dorn, M.; Kalmbach, J.; Boden, P.; Päpcke, A.; Gómez, S.; Förster, C.; Kuczelinis, F.; Carrella, L. M.; Büldt, L. A.; Bings, N. H.; Rentschler, E.; Lochbrunner, S.; González, L.; Gerhards, M.; Seitz, M.; Heinze, K. A Vanadium(III) Complex with Blue and NIR-II Spin-Flip Luminescence in Solution. *J. Am. Chem. Soc.* **2020**, *142* (17), 7947 – 7955. DOI: 10.1021/jacs.0c02122.

(16) Fataftah, M. S.; Bayliss, S. L.; Laorenza, D. W.; Wang, X.; Phelan, B. T.; Wilson, C. B.; Mintun, P. J.; Kovos, B. D.; Wasielewski, M. R.; Han, S.; Sherwin, M. S.; Awschalom, D. D.; Freedman, D. E. Trigonal Bipyramidal V3+ Complex as an Optically Addressable Molecular Qubit Candidate. *J. Am. Chem. Soc.* **2020.** DOI: 10.1021/jacs.0c08986.

(17) Dorn, M.; Kalmbach, J.; Boden, P.; Kruse, A.; Dab, C.; Reber, C.; Niedner-Schatteburg, G.; Lochbrunner, S.; Gerhards, M.; Seitz, M.; Heinze, K. Ultrafast and long-time excited state kinetics of an NIR-emissive vanadium(iii) complex I: synthesis, spectroscopy and static quantum chemistry. *Chem. Sci.* **2021**, *12* (32), 10780 – 10790. DOI: 10.1039/D1SC02137K.

(18) Zobel, J. P.; Knoll, T.; González, L. Ultrafast and long-time excited state kinetics of an NIR-emissive vanadium(iii) complex II. Elucidating triplet-to-singlet excited-state dynamics. *Chem. Sci.* **2021**, *12* (32), 10791 – 10801. DOI: 10.1039/D1SC02149D.

(19) Otto, S.; Grabolle, M.; Förster, C.; Kreitner, C.; Resch-Genger, U.; Heinze, K. Cr(ddpd)2(3+) A Molecular, Water-Soluble, Highly NIR-Emissive Ruby Analogue. *Angew. Chem. Int. Ed.* **2015**, *54* (39), 11572 – 11576. DOI: 10.1002/anie.201504894.

(20) Jiménez, J.-R.; Poncet, M.; Míguez-Lago, S.; Grass, S.; Lacour, J.; Besnard, C.; Cuerva, J. M.; Campaña, A. G.; Piguet, C. Bright Long-Lived Circularly Polarized Luminescence in Chiral Chromium(III) Complexes. *Angew. Chem. Int. Ed.* **2021**, *60* (18), 10095 – 10102. DOI: 10.1002/anie.202101158.

(21) Sinha, N.; Jiménez, J.-R.; Pfund, B.; Prescimone, A.; Piguet, C.; Wenger, O. S. A Near-Infrared-II Emissive Chromium(III) Complex. *Angew. Chem. Int. Ed.* **2021.** DOI: 10.1002/anie.202106398.

(22) Wang, C.; Reichenauer, F.; Kitzmann, W. R.; Kerzig, C.; Heinze, K.; Resch-Genger, U. Efficient Triplet-Triplet Annihilation Upconversion Sensitized by a Chromium(III) Complex via an Underexplored Energy Transfer Mechanism. *Angew. Chem. Int. Ed.* **2022**, *61* (27), e202202238. DOI: 10.1002/anie.202202238.

(23) Wegeberg, C.; Häussinger, D.; Wenger, O. S. Pyrene-Decoration of a Chromium(0) Tris(diisocyanide) Enhances Excited State Delocalization: A Strategy to Improve the Photoluminescence of 3d6 Metal Complexes. *J. Am. Chem. Soc.* **2021**, *143* (38), 15800 – 15811. DOI: 10.1021/jacs.1c07345.

(24) Reichenauer, F.; Wang, C.; Förster, C.; Boden, P.; Ugur, N.; Báez-Cruz, R.; Kalmbach, J.; Carrella, L. M.; Rentschler, E.; Ramanan, C.; Niedner-Schatteburg, G.; Gerhards, M.; Seitz, M.; Resch-Genger, U.; Heinze, K. Strongly Red-Emissive Molecular Ruby Cr(bpmp)23+ Surpasses Ru(bpy)32. *J. Am. Chem. Soc.* **2021**, *143* (30), 11843 – 11855. DOI: 10.1021/jacs.1c05971.

(25) Kitzmann, W. R.; Ramanan, C.; Naumann, R.; Heinze, K. Molecular ruby: exploring the excited state landscape. *Dalton Trans.* **2022.** DOI: 10.1039/d2dt00569g.

(26) Sittel, S.; Naumann, R.; Heinze, K. Molecular Rubies in Photoredox Catalysis. *Front. Chem.* **2022**, *10*, 887439. DOI: 10.3389/fchem.2022.887439.

(27) Kjær, K. S.; Kaul, N.; Prakash, O.; Chábera, P.; Rosemann, N. W.; Honarfar, A.; Gordivska, O.; Fredin, L. A.; Bergquist, K.-E.; Häggström, L.; Ericsson, T.; Lindh, L.; Yartsev, A.; Styring, S.; Huang, P.; Uhlig, J.; Bendix, J.; Strand, D.; Sundström, V.; Persson, P.; Lomoth, R.; Wärnmark, K. Luminescence and reactivity of a charge-transfer excited iron complex with nanosecond lifetime. *Science* **2019**, *363* (6424), 249 – 253. DOI: 10.1126/science.aau7160.

(28) Dierks, P.; Vukadinovic, Y.; Bauer, M. Photoactive iron complexes: more sustainable, but still a challenge. *Inorg. Chem. Front.* **2022**, *9* (2), 206 – 220. DOI: 10.1039/D1QI01112J.
(29) Leis, W.; Argüello Cordero, M. A.; Lochbrunner, S.; Schubert, H.; Berkefeld, A. A Photoreactive Iron(II) Complex Luminophore. *J. Am. Chem. Soc.* **2022**, *144* (3), 1169 – 1173. DOI: 10.1021/jacs.1c13083.
(30) Harris, J. P.; Reber, C.; Colmer, H. E.; Jackson, T. A.; Forshaw, A. P.; Smith, J. M.; Kinney, R. A.; Telser, J. Near-infrared 2 E g → 4 A 2g and visible LMCT luminescence from a molecular bis -(tris(carbene)borate) manganese(IV) complex. *Can. J. Chem.* **2017**, *95* (5), 547 – 552. DOI: 10.1139/cjc-2016-0607.
(31) Herr, P.; Kerzig, C.; Larsen, C. B.; Häussinger, D.; Wenger, O. S. Manganese(I) complexes with metal-to-ligand charge transfer luminescence and photoreactivity. *Nat. Chem.* **2021.** DOI: 10.1038/s41557-021-00744-9.
(32) East, N.; Naumann, R.; Förster, C.; Ramanan, C.; Diezemann, G.; Heinze, K. *Oxidative Two-State Photoreactivity of a Manganese(IV) Complex using NIR Light*, 2023. DOI: 10.26434/chemrxiv-2023-bhl82.
(33) Kaufhold, S.; Rosemann, N. W.; Chábera, P.; Lindh, L.; Bolaño Losada, I.; Uhlig, J.; Pascher, T.; Strand, D.; Wärnmark, K.; Yartsev, A.; Persson, P. Microsecond Photoluminescence and Photoreactivity of a Metal-Centered Excited State in a Hexacarbene-Co(III) Complex. *J. Am. Chem. Soc.* **2021**, *143* (3), 1307 – 1312. DOI: 10.1021/jacs.0c12151.
(34) Sinha, N.; Pfund, B.; Wegeberg, C.; Prescimone, A.; Wenger, O. S. Cobalt(III) Carbene Complex with an Electronic Excited-State Structure Similar to Cyclometalated Iridium(III) Compounds. *J. Am. Chem. Soc.* **2022**, *144* (22), 9859 – 9873. DOI: 10.1021/jacs.2c02592.
(35) Hossain, A.; Bhattacharyya, A.; Reiser, O. Copper's rapid ascent in visible-light photoredox catalysis. *Science* **2019**, *364* (6439). DOI: 10.1126/science.aav9713.
(36) Hamze, R.; Peltier, J. L.; Sylvinson, D.; Jung, M.; Cardenas, J.; Haiges, R.; Soleilhavoup, M.; Jazzar, R.; Djurovich, P. I.; Bertrand, G.; Thompson, M. E. Eliminating nonradiative decay in Cu(I) emitters: 99% quantum efficiency and microsecond lifetime. *Science* **2019**, *363* (6427), 601 – 606. DOI: 10.1126/science.aav2865.
(37) Beaudelot, J.; Oger, S.; Peruško, S.; Phan, T.-A.; Teunens, T.; Moucheron, C.; Evano, G. Photoactive Copper Complexes: Properties and Applications. *Chem. Rev.* **2022**, *122* (22), 16365 – 16609. DOI: 10.1021/acs.chemrev.2c00033.
(38) Büldt, L. A.; Guo, X.; Prescimone, A.; Wenger, O. S. A Molybdenum(0) Isocyanide Analogue of Ru(2,2'-Bipyridine)3 (2+) : A Strong Reductant for Photoredox Catalysis. *Angew. Chem. Int. Ed.* **2016**, *55* (37), 11247 – 11250. DOI: 10.1002/anie.201605571.
(39) Herr, P.; Schwab, A.; Kupfer, S.; Wenger, O. S. Deep-Red Luminescent Molybdenum(0) Complexes with Bi- and Tridentate Isocyanide Chelate Ligands. *ChemPhotoChem* **2022.** DOI: 10.1002/cptc.202200052.
(40) Boden, P.; Di Martino-Fumo, P.; Bens, T.; Steiger, S.; Albold, U.; Niedner-Schatteburg, G.; Gerhards, M.; Sarkar, B. NIR Emissive Chromium(0), Molybdenum(0) and Tungsten(0) Complexes in the Solid State at Room Temperature. *Chem. Eur. J.* **2021.** DOI: 10.1002/chem.202102208.
(41) Bilger, J. B.; Kerzig, C.; Larsen, C. B.; Wenger, O. S. A Photorobust Mo(0) Complex Mimicking Os(2,2'-bipyridine)32+ and Its Application in Red-to-Blue Upconversion. *J. Am. Chem. Soc.* **2021**, *143* (3), 1651 – 1663. DOI: 10.1021/jacs.0c12805.
(42) Gowda, A. S.; Petersen, J. L.; Milsmann, C. Redox Chemistry of Bis(pyrrolyl)pyridine Chromium and Molybdenum Complexes: An Experimental and Density Functional Theoretical Study. *Inorg. Chem.* **2018**, *57* (4), 1919 – 1934. DOI: 10.1021/acs.inorgchem.7b02809.
(43) Kübler, J. A.; Pfund, B.; Wenger, O. S. Zinc(II) Complexes with Triplet Charge-Transfer Excited States Enabling Energy-Transfer Catalysis, Photoinduced Electron Transfer, and Upconversion. *JACS Au* **2022**, *2* (10), 2367 – 2380. DOI: 10.1021/jacsau.2c00442.
(44) Mrózek, O.; Mitra, M.; Hupp, B.; Belyaev, A.; Lüdtke, N.; Wagner, D.; Wang, C.; Wenger, O. S.; Marian, C. M.; Steffen, A. An Air- and Moisture-stable Zinc(II) Carbene Dithiolate Dimer Showing Fast Thermally Activated Delayed Fluorescence and Dexter Energy Transfer Catalysis. *Chem. Eur. J.* **2023.** DOI: 10.1002/chem.202203980.
(45) Bell, J. D.; Murphy, J. A. Recent advances in visible light-activated radical coupling reactions triggered by (i) ruthenium, (ii) iridium and (iii) organic photoredox agents. *Chem. Soc. Rev.* **2021**, *50* (17), 9540 – 9685. DOI: 10.1039/D1CS00311A.
(46) Arias-Rotondo, D. M. The fruit fly of photophysics. *Nat. Chem.* **2022**, *14* (6), 716. DOI: 10.1038/s41557-022-00955-8.
(47) Arias-Rotondo, D. M.; McCusker, J. K. An Overview of the Physical and Photophysical Properties of [Ru(bpy) 3] 2+. In *Visible Light Photocatalysis in Organic Chemistry*; Stephenson, C., Yoon, T., MacMillan, D. W. C., Eds.; Wiley-VCH Verlag GmbH & Co. KGaA, 2018; pp 1 – 24. DOI: 10.1002/9783527674145.ch1.
(48) Liu, Z.; Bian, Z.; Huang, C. Luminescent Iridium Complexes and Their Applications. In *Molecular Organometallic Materials for Optics*; Bozec, H., Guerchais, V., Eds.; Topics in Organometallic Chemistry; Springer Berlin Heidelberg, 2010; pp 113 – 142. DOI: 10.1007/978-3-642-01866-4_4.
(49) Chou, P.-T.; Chi, Y. Osmium- and Ruthenium-Based Phosphorescent Materials: Design, Photophysics, and Utilization in OLED Fabrication. *Eur. J. Inorg. Chem.* **2006**, *2006* (17), 3319 – 3332. DOI: 10.1002/ejic.200600364.
(50) Herr, P.; Glaser, F.; Büldt, L. A.; Larsen, C. B.; Wenger, O. S. Long-Lived, Strongly Emissive, and Highly Reducing Excited States in Mo(0) Complexes with Chelating Isocyanides. *J. Am. Chem. Soc.* **2019**, *141* (36), 14394 – 14402. DOI: 10.1021/jacs.9b07373.
(51) Ardon, M.; Hogarth, G.; Oscroft, D. T. Organometallic chemistry in a conventional microwave oven: the facile synthesis of group 6 carbonyl complexes. *J. Organomet. Chem.* **2004**, *689* (15), 2429 – 2435. DOI: 10.1016/j.jorganchem.2004.04.030.
(52) Manuta, D. M.; Lees, A. J. Emission and photochemistry of M(CO)4(diimine) (M = chromium, molybdenum, tungsten) complexes in room-temperature solution. *Inorg. Chem.* **1986**, *25* (9), 1354 – 1359. DOI: 10.1021/ic00229a012.
(53) Manuta, D. M.; Lees, A. J. Solvent and substituent effects on the lowest energy excited states of M(CO)4(diimine) (M = Cr, Mo, W) complexes. *Inorg. Chem.* **1983**, *22* (25), 3825 – 3828. DOI: 10.1021/ic00167a031.
(54) Boden, P. J.; Di Martino-Fumo, P.; Bens, T.; Steiger, S. T.; Marhöfer, D.; Niedner-Schatteburg, G.; Sarkar, B. Mechanistic and Kinetic Investigations of ON/OFF (Photo)Switchable Binding of Carbon Monoxide by Chromium(0), Molybdenum(0) and Tungsten(0) Carbonyl Complexes with a Pyridyl-Mesoionic Carbene Ligand. *Chem. Eur. J.* **2022**, *28* (51), e202201038. DOI: 10.1002/chem.202201038.
(55) Boden, P. J.; Di Martino-Fumo, P.; Bens, T.; Steiger, S. T.; Marhöfer, D.; Niedner-Schatteburg, G.; Sarkar, B. Mechanistic and Kinetic Investigations of ON/OFF (Photo)Switchable Binding of Carbon Monoxide by Chromium(0), Molybdenum(0) and Tungsten(0) Carbonyl Complexes with a Pyridyl-Mesoionic Carbene Ligand. *Chemistry (Weinheim an der Bergstrasse, Germany)* **2022**, *28* (51), e202202543. DOI: 10.1002/chem.202202543.
(56) Tang, M.; Cameron, L.; Poland, E. M.; Yu, L.-J.; Moggach, S. A.; Fuller, R. O.; Huang, H.; Sun, J.; Thickett, S. C.; Massi, M.; Coote, M. L.; Ho, C. C.; Bissember, A. C. Photoactive Metal Carbonyl Complexes Bearing N-Heterocyclic Carbene Ligands: Synthesis, Characterization, and Viability as Photoredox Catalysts. *Inorg. Chem.* **2022**, *61* (4), 1888 – 1898. DOI: 10.1021/acs.inorgchem.1c02964.
(57) Gade, L. H. *Koordinationschemie*, 1st ed.; Wiley, 1998. DOI: 10.1002/9783527663927.
(58) Kunkely, H.; Vogler, A. Excited state properties of the (tropylium)molybdenum tricarbonyl cation. *Chem. Commun.* **1998** (3), 397 – 398. DOI: 10.1039/A706767D.
(59) Faller, J. W.; Ma, Y. Strong Lewis acids derived from molybdenum and tungsten nitrosyls containing the tri-2-pyridylmethane ligand. Dynamic NMR studies of their adducts with aldehydes, ke-

tones, and esters. *J. Am. Chem. Soc.* **1991**, *113* (5), 1579 – 1586. DOI: 10.1021/ja00005a021.
(60) García, F.; Hopkins, A. D.; Kowenicki, R. A.; McPartlin, M.; Rogers, M. C.; Silvia, J. S.; Wright, D. S. Syntheses and Structure of Heterometallic Complexes Containing Tripodal Group 13 Ligands [RE(2-py) 3] - (E = Al, In). *Organometallics* **2006**, *25* (10), 2561 – 2568. DOI: 10.1021/om0600691.
(61) Kuo, C.-Y.; Fuh, Y.-S.; Shiue, J.-Y.; Joyce Yu, S.; Lee, G.-H.; Peng, S.-M. Syntheses and chemistry of Tris(2-pyridyl)phosphine complexes of Group VI transition metals. X-ray structural studies of the molybdenum complexes. *J. Organomet. Chem.* **1999**, *588* (2), 260 – 267. DOI: 10.1016/S0022-328X(99)00387-3.
(62) Morales, D.; Pérez, J.; Riera, L.; Riera, V.; Miguel, D. Molybdenum and Tungsten Tricarbonyl Complexes with the Tripodal Ligands [n BuSn(2-pyridyl) 3] and [RSn(methylthiomethyl) 3]. *Organometallics* **2001**, *20* (22), 4517 – 4523. DOI: 10.1021/om0104722.
(63) Hanf, S.; Colebatch, A. L.; Stehr, P.; García-Rodríguez, R.; Hey-Hawkins, E.; Wright, D. S. An experimental and theoretical study of the coordination and donor properties of tris-2-pyridylphosphine ligands. *Dalton Trans.* **2020**, *49* (16), 5312 – 5322. DOI: 10.1039/D0DT00609B.
(64) Santoro, A.; Sambiagio, C.; McGowan, P. C.; Halcrow, M. A. Synthesis and coordination chemistry of 1,1,1-tris-(pyrid-2-yl)ethane. *Dalton Trans.* **2015**, *44* (3), 1060 – 1069. DOI: 10.1039/c4dt02824d.
(65) Elschenbroich, C. *Organometallchemie*, 6., überarbeitete Auflage; Lehrbuch Chemie; Teubner, 2008.
(66) Janiak, C. A critical account on π – π stacking in metal complexes with aromatic nitrogen-containing ligands †. *J. Chem. Soc., Dalton Trans.* **2000** (21), 3885 – 3896. DOI: 10.1039/b003010o.
(67) Braga, S. S.; Coelho, A. C.; Gonçalves, I. S.; Almeida Paz, F. A. (2,2′-Bipyridine)tetracarbonylmolybdenum(0). *Acta Crystallogr. E* **2007**, *63* (3), m780-m782. DOI: 10.1107/S1600536807007234.
(68) Ogata, K.; Yamaguchi, Y.; Kurihara, Y.; Ueda, K.; Nagao, H.; Ito, T. Twisted coordination mode of bis(N-heterocyclic carbene) ligands in octahedral geometry of group 6 transition metal complexes: Synthesis, structure, and reactivity. *Inorg. Chim. Acta* **2012**, *390*, 199 – 209. DOI: 10.1016/j.ica.2012.04.027.
(69) Reichardt, C. Solvatochromic Dyes as Solvent Polarity Indicators. *Chem. Rev.* **1994**, *94* (8), 2319 – 2358. DOI: 10.1021/cr00032a005.
(70) Plasser, F. TheoDORE: A toolbox for a detailed and automated analysis of electronic excited state computations. *J. Chem. Phys.* **2020**, *152* (8), 84108. DOI: 10.1063/1.5143076.
(71) Burgess, J. Solvent effects on the visible absorption spectra of Mo(CO)4(Bipy) and W(CO)4(Bipy). *J. Organomet. Chem.* **1969**, *19* (1), 218 – 220. DOI: 10.1016/S0022-328X(00)87776-1.
(72) Nigam, S.; Rutan, S. Principles and Applications of Solvatochromism. *Appl. Spectrosc.* **2001**, *55* (11), 362A-370A. DOI: 10.1366/0003702011953702.
(73) Suzuki, K.; Kobayashi, A.; Kaneko, S.; Takehira, K.; Yoshihara, T.; Ishida, H.; Shiina, Y.; Oishi, S.; Tobita, S. Reevaluation of absolute luminescence quantum yields of standard solutions using a spectrometer with an integrating sphere and a back-thinned CCD detector. *Phys. Chem. Chem. Phys.* **2009**, *11* (42), 9850 – 9860. DOI: 10.1039/b912178a.
(74) Lees, A. J. Luminescence properties of organometallic complexes. *Chem. Rev.* **1987**, *87* (4), 711 – 743. DOI: 10.1021/cr00080a003.
(75) Rawlins, K. A.; Lees, A. J. Photophysical properties of M(CO)4(.alpha.,.alpha.'-diimine) (M = molybdenum, tungsten) complexes. *Inorg. Chem.* **1989**, *28* (11), 2154 – 2160. DOI: 10.1021/ic00310a028.
(76) Wrighton, M.; Morse, D. L. Nature of the lowest excited state in tricarbonylchloro-1,10-phenanthrolinerhenium(I) and related complexes. *J. Am. Chem. Soc.* **1974**, *96* (4), 998 – 1003. DOI: 10.1021/ja00811a008.
(77) Moll, J.; Wang, C.; Päpcke, A.; Förster, C.; Resch-Genger, U.; Lochbrunner, S.; Heinze, K. Green-Light Activation of Push-Pull Ruthenium(II) Complexes. *Chem. Eur. J.* **2020**, *26* (30), 6820 – 6832. DOI: 10.1002/chem.202000871.
(78) Wenger, O. S. Is Iron the New Ruthenium? *Chem. Eur. J.* **2019**, *25* (24), 6043 – 6052. DOI: 10.1002/chem.201806148.
(79) Hager, G. D.; Crosby, G. A. Charge-transfer exited states of ruthenium(II) complexes. I. Quantum yield and decay measurements. *J. Am. Chem. Soc.* **1975**, *97* (24), 7031 – 7037. DOI: 10.1021/ja00857a013.
(80) van Houten, J.; Watts, R. J. Temperature dependence of the photophysical and photochemical properties of the tris(2,2'-bipyridyl)ruthenium(II) ion in aqueous solution. *J. Am. Chem. Soc.* **1976**, *98* (16), 4853 – 4858. DOI: 10.1021/ja00432a028.
(81) Goez, M.; Kerzig, C.; Naumann, R. An "all-green" catalytic cycle of aqueous photoionization. *Angew. Chem. Int. Ed.* **2014**, *53* (37), 9914 – 9916. DOI: 10.1002/anie.201405693.
(82) Kerzig, C.; Goez, M. Combining energy and electron transfer in a supramolecular environment for the "green" generation and utilization of hydrated electrons through photoredox catalysis. *Chem. Sci.* **2016**, *7* (6), 3862 – 3868. DOI: 10.1039/C5SC04800A.
(83) Müller, P.; Brettel, K. Ru(bpy)(3)(2+) as a reference in transient absorption spectroscopy: differential absorption coefficients for formation of the long-lived (3)MLCT excited state. *Photochem. Photobiol. Sci.* **2012**, *11* (4), 632 – 636. DOI: 10.1039/C2PP05333K.
(84) Demas, J. N.; Taylor, D. G. On the "intersystem crossing" yields in ruthenium(II) and osmium(II) photosensitizers. *Inorg. Chem.* **1979**, *18* (11), 3177 – 3179. DOI: 10.1021/ic50201a044.
(85) Cannizzo, A.; van Mourik, F.; Gawelda, W.; Zgrablic, G.; Bressler, C.; Chergui, M. Broadband femtosecond fluorescence spectroscopy of Ru(bpy)32+. *Angew. Chem.* **2006**, *118*, 3246 – 3248. *Angew. Chem. Int. Ed.* **2006**, *45* (19), 3174 – 3176. DOI: 10.1002/anie.200600125.
(86) Wright, M. A.; Wright, J. A. PhotoCORMs: CO release moves into the visible. *Dalton Trans.* **2016**, *45* (16), 6801 – 6811. DOI: 10.1039/C5DT04849D.
(87) Schmid, L.; Kerzig, C.; Prescimone, A.; Wenger, O. S. Photostable Ruthenium(II) Isocyanoborato Luminophores and Their Use in Energy Transfer and Photoredox Catalysis. *JACS Au* **2021**, *1* (6), 819 – 832. DOI: 10.1021/jacsau.1c00137.
(88) Uji, M.; Zähringer, T. J. B.; Kerzig, C.; Yanai, N. Visible-to-UV Photon Upconversion: Recent Progress in New Materials and Applications. *Angew. Chem. Int. Ed.* **2023**, e202301506. DOI: 10.1002/anie.202301506.
(89) Haefele, A.; Blumhoff, J.; Khnayzer, R. S.; Castellano, F. N. Getting to the (Square) Root of the Problem: How to Make Noncoherent Pumped Upconversion Linear. *J. Phys. Chem. Lett.* **2012**, *3* (3), 299 – 303. DOI: 10.1021/jz300012u.
(90) Chattopadhyay, S. K.; Kumar, C.; Das, P. K. Triplet-related photophysics of 9,10-diphenylanthracene. A kinetic study of reversible energy transfer from anthracene triplet by nanosecond laser flas. *Chem. Phys. Lett.* **1983**, *98* (3), 250 – 254. DOI: 10.1016/0009-2614(83)87160-7.
(91) Montalti, M.; Murov, S. L. *Handbook of photochemistry*, 3rd ed.; CRC/Taylor & Francis, 2006.
(92) Kerzig, C.; Wenger, O. S. Sensitized triplet-triplet annihilation upconversion in water and its application to photochemical transformations. *Chem. Sci.* **2018**, *9* (32), 6670 – 6678. DOI: 10.1039/C8SC01829D.
(93) Naumann, R.; Goez, M. How the sustainable solvent water unleashes the photoredox catalytic potential of ruthenium polypyridyl complexes for pinacol couplings. *Green Chem.* **2019**, *21* (16), 4470 – 4474. DOI: 10.1039/C9GC02069A.
(94) Gimeno, L.; Queffélec, C.; Mall Haidaraly, K.; Blart, E.; Pellegrin, Y. Dehalogenation reaction photocatalyzed by homoleptic copper(i) complexes associated with strongly reductive sacrificial donors. *Catal. Sci. Technol.* **2021**, *11* (18), 6041 – 6047. DOI: 10.1039/D1CY01209F.

(95) Connelly, N. G.; Geiger, W. E. Chemical Redox Agents for Organometallic Chemistry. *Chem. Rev.* **1996**, *96* (2), 877 – 910. DOI: 10.1021/cr940053x.
(96) Chun, S.; Getty, E. G.; Lees, A. J. Photophysics of metal carbonyl complexes. Excited states of a series of cis-M(CO)4L2 complexes (M = Cr, Mo, or W; L = pyridine or a pyridine derivative). *Inorg. Chem.* **1984**, *23* (14), 2155 – 2160. DOI: 10.1021/ic00182a034.
(97) Connor, J. A.; Overton, C.; El Murr, N. Electronic spectra and electrochemistry of disubstituted 2,2′-bipyridinetetracarbonylmolybdenum complexes. Solvent and substituent effects. *J. Organomet. Chem.* **1984**, *277* (2), 277 – 284. DOI: 10.1016/0022-328X(84)80709-3.

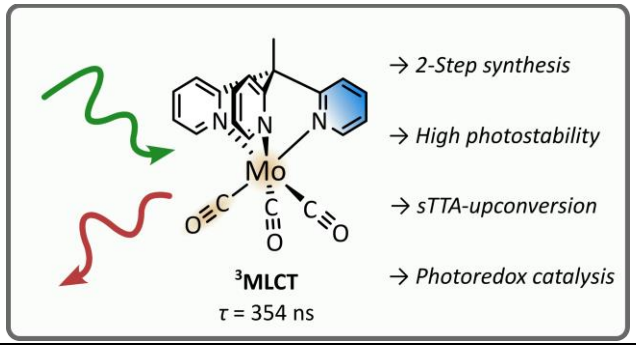
→ 2-Step synthesis
→ High photostability
→ sTTA-upconversion
→ Photoredox catalysis
Mo
N
N
N
C
O
C
O
C
O
³MLCT
τ = 354 ns